applied sciences

MDPI

Article

Duration of Rainfall Fades in GeoSurf Satellite Constellations

Emilio Matricciani * and Carlo Riva

Dipartimento di Elettronica, Informazione e Bioingegneria (DEIB), Politecnico di Milano, 20133 Milan, Italy; carlo.riva@polimi.it

* Correspondence: emilio.matricciani@polimi.it

Abstract: We have studied the stochastic processes A and B concerning fade durations due to rain, by simulating attenuation time series $A(t)$ (dB) in the zenith paths of GeoSurf satellite constellations, at sites located in different climatic regions, with the Synthetic Storm Technique. Process B gives the statistics of outages (occurrences) and process A gives the statistics of outage duration (fraction of time), for the same rain attenuation threshold $A(t) > S$. The two processes are not independent; therefore, we have studied the relationship between their probabilities and defined a uniformity index $0 < U(S) \leq 1$. $U(S)$ is useful for comparing real cases–fade durations fragmented in many different intervals, with changing S and site—and the limiting case of all fades lasting the same time. As S increases, $U(S)$ increases, approaching 1 at very large thresholds. These results should guide the designers of satellite constellations to consider the impact of $A(t)$ on diverse communications services. Process B (occurrences) impacts mainly on non–real-time services, such as data delivery, more disturbed by the number of outages rather than by their duration. Process A (fraction of time) impacts mainly on real–time services such as television, video conference etc., more disturbed by the duration of the outage.

Keywords: attenuation; fade duration; GeoSurf; millimeter waves; outage; rainfall; satellite constellation; uniformity index

Citation: Matricciani, E.; Riva, C. Duration of Rainfall Fades in GeoSurf Satellite Constellations. *Appl. Sci.* **2024**, *14*, 1865. https://doi.org/10.3390/app14051865

Academic Editor: John Xiupu Zhang

Received: 30 January 2024
Revised: 9 February 2024
Accepted: 21 February 2024
Published: 24 February 2024

1. GeoSurf Satellite Constellations at Millimeter Wavelengths

GeoSurf constellations [1] share most of the advantages of current GEO (Geostationary), MEO (Medium Earth Orbit) and LEO (Low Earth Orbit) satellite constellations, without suffering most of the drawbacks of these designs, because GeoSurf uses zenith radio propagation paths worldwide; therefore, it is as if the site were at the equator and connecting to a GEO satellite at the zenith.

In [2], we studied the tropospheric attenuation of GeoSurf zenith paths and compared it to that of the slant paths to GEO, MEO and LEO satellites. In [3], we studied the annual average probability distribution $P(A)$ of exceeding rain attenuation A (dB), and showed how it depends on carrier frequency at sites located in different climatic regions (sites also considered in the present paper). As experimental results, we considered the rain attenuation time series $A(t)$ simulated with the Synthetic Storm Technique (SST) [4] from on–site rain rate time series $R(t)$ recorded for several years.

Because these studies refer to channels with negligible linear (amplitude and phase) distortions—i.e., narrow–band channels–in [5], we simulated the slowly time–varying transfer–function and linear distortions in ultra–wideband radio links in GeoSurf constellations working at millimeter wavelengths, namely 80 GHz in 10-GHz bandwidth channels. We think that these channels can be used in future worldwide internet, adopting spread spectrum modulation and code division multiple access (CDMA) [6–10], with BPSK and QPSK modulation. In fact, CDMA can provide a large processing gain, it is robust against frequency interference and it does not require multiple access coordination (all characteristics which, together with the further advantages of the GeoSurf constellations concerning

radio propagation, mentioned in Table 1 of [1], make it an effective choice to provide high bit rates to scattered users).

Table 1. Geographical coordinates, altitude (km), number of years of continuous rain rate time series measurements at the indicated sites.

Site	Latitude N (°)	Longitude E (°)	Altitude H_S (m)	Rain Rate Observation Time (Years)
Spino d'Adda (Italy)	45.4	9.5	84	8
Gera Lario (Italy)	46.2	9.4	210	5
Fucino (Italy)	42.0	13.6	680	5
Madrid (Spain)	40.4	356.3	630	8
Prague (Czech Republic)	50.0	14.5	250	5
Tampa (Florida)	28.1	277.6	50	4
Norman (Oklahoma)	35.2	262.6	420	4
White Sands (New Mexico)	32.5	253.4	1463	5
Vancouver (British Columbia)	49.2	236.8	80	3

Continuing our development of GeoSurf satellite constellations design, in [11], we studied the interference caused by amplitude and phase distortions induced by rain (simulations with the SST) in ultra–wideband communication systems designed for using amplitude modulation. We have shown that the theoretical capacity loss of these channels is small; therefore, they can be used at millimeter waves.

In the present paper, our aim is to study fade durations at millimeter waves by simulating rain attenuation time series $A(t)$ at 80 GHz, with the SST, from long–term on–site recordings of rain rate time series $R(t)$.

Fade duration is the second most important link parameter required for designing a satellite link faded by rain because it gives the interval $A(t)$ exceeds an attenuation threshold S (dB) (usually, the link power margin compared to clear sky). The first is the probability of exceeding the link power margin, with no information on its duration. Therefore, fade durations have been measured, at lower frequency bands, in several satellite links, as reported in more recent references [12–27], in slant paths not larger than about 60°, as in the ITU–R Recommendation [28].

No measurements or predictions are, however, available for zenith paths, even when low–latitude sites are considered [16]. Now, the SST is a powerful tool that can simulate reliable time series $A(t)$ in slant paths in which simulations of fade duration statistics were validated years ago [29] and more recently [22].

Figure 1 shows $A(t)$ at 80 GHz, circular polarization, simulated in the zenith path at Spino d'Adda (Table 1). A threshold S (dB) can be crossed more than once, with different intervals τ (min) which define the stochastic variable "fade duration". Since S is usually the power margin of the radio link, any time $A(t) > S$, the communication link fades and the communication system experiences an outage.

We can count the number of these occurrences and calculate the outage probability. Long ago, we called this stochastic process "process B" [30]. However, besides the number of occurrences, the duration τ itself is also another stochastic variable of great importance because it gives the outage duration. We called this process of fade duration "process A" [30].

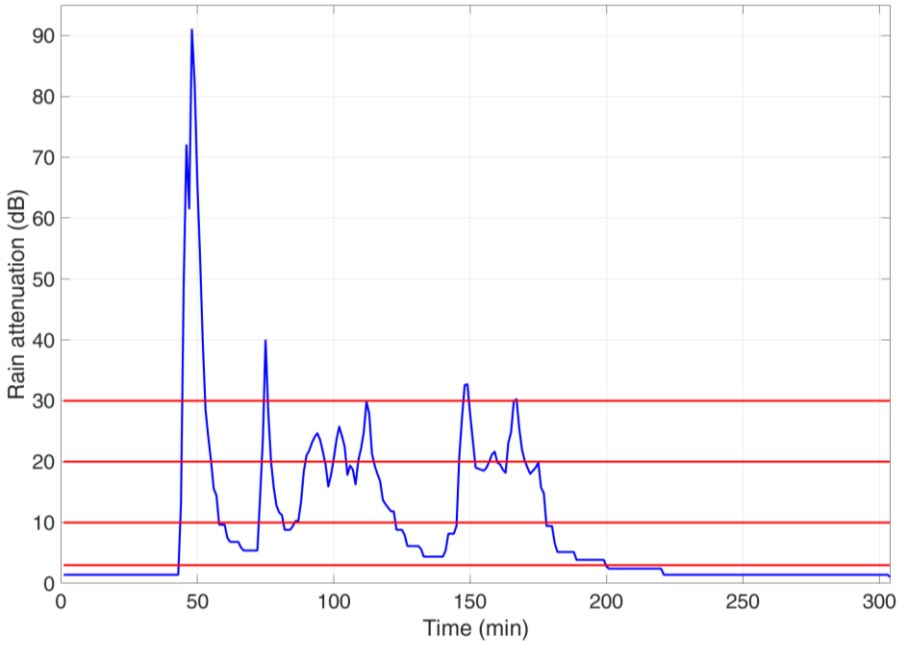

Figure 1. Rain attenuation time series (blue line), 80 GHz circular polarization, zenith path, at Spino d'Adda, 6 May 2000, rain event starts at 17:30 local time. The red lines are drawn at thresholds 3, 10, 20 and 30 dB.

In other words, process B gives the statistics of outages, process A gives the statistics of outage duration. In satellite communications, both are, of course, useful because some services–especially non–real-time services, such as data delivery–can be more disturbed by the number of outages (e.g., in an average year, month, etc.) rather than by their duration, while some others–especially real–time services such as television, video conference etc.–are more disturbed by the duration of the outage.

In the next section, we define the probability distribution of the processes A and B; in Section 3, we present worldwide sites investigated with the Synthetic Storm Technique; in Section 4, we show the fade duration experimental results; in Section 5, we study the interdependence of the two processes; in Section 6, we define and study a uniformity index, which compares real cases–fade durations fragmented in many different intervals, with changing S and site–to the limiting case of all fades lasting the same time; finally, in Section 7, we conclude by summarizing the main results and their impact on system design.

2. Fade Duration Processes A and B

According to [30], fade duration can be studied from two points of view, both useful. The stochastic variable is the same for both processes–namely the interval τ in which $A(t) > S$ continuously–but the statistical "weight" given to τ is different. In process A, an interval τ is given a weight τ, while in process B, it is given a weight of one unit. This approach of distinguishing and studying the two processes is very fruitful when a stocastic variable assumes values in a large range–as it occurs for rainfall fades–and when they impact on a system differently, according to the interruptions tolerated by users.

The conditional cumulative probability distribution of exceeding a fade duration D in process A, $P_{S,A}(\tau > D) = P_{S,A}(D)$, is defined by:

$$P_{S,A}(\tau > D) = 1 - P_{S,A}(\tau \leq D) = 1 - \int_0^D n(\tau) \times \tau d\tau / T_S \quad (1)$$

In Equation (1), $n(\tau)$ is the number of fades of duration τ, $T_S = \int_0^\infty \tau d\tau$ is the total time the threshold S is exceeded in the reference time (e.g., in an average year, month, etc.)

According to Equation (1), $P_{S,A}(D)$ can be also read as the fraction of the total time T_S for which $A(t) > S$.

The conditional cumulative probability distribution of exceeding D in process B, $P_{S,B}(\tau > D) = P_{S,B}(D)$, is defined by:

$$P_{S,B}(\tau > D) = 1 - P_{S,B}(\tau \leq D) = 1 - \int_0^{n(D)} n(\tau) dn(\tau) / N(S) \quad (2)$$

In Equation (2), $N(S) = \int_0^{\infty} n(\tau) d(n(\tau))$ is the total number of fade durations the threshold S is exceeded in the reference time. According to Equation (2), $P_{S,B}(D)$ is read in the usual way of percentage of total occurrences $N(S)$ for which $A(t) > S$. In both equations, the integrals are calculated as discrete summations.

3. Worldwide Sites Investigated with the Synthetic Storm Technique

To illustrate the general characteristics of $P_{S,A}(D)$ and $P_{S,B}(D)$ and their relationship, we report the results concerning the sites listed in Table 1, located in different climatic regions. The rain attenuation expected in GeoSurf radio—links is independent of the particular GeoSurf design (e.g., altitude and number of satellites), because all paths to/from a satellite of the constellation are always vertical (zenith paths) [1]. $A(t)$ is calculated with the Synthetic Storm Technique [4].

Besides being in different climatic regions, these particular sites are useful study–cases because: (a) On–site rain—rate time series $R(t)$ (mm/h)—the input physical measurements to the SST [4]—with rain rate averaged in 1 min intervals, were continuously recorded for several years; (b) They are the sites of important NASA and ESA satellite ground stations (Fucino, Madrid, White Sands), or the site where long–term radio propagation experiments were performed in Italy (Fucino, Gera Lario, Spino d'Adda) or large cities (Prague, Norman, Tampa, Vancouver).

Figure 2 shows the average annual probability distribution $P(R)$ of exceeding R (mm/h, averaged in 1 min) measured at the indicated sites. The different climatic rain conditions of these sites are clearly evident by comparing the rain rate exceeded with the same probability.

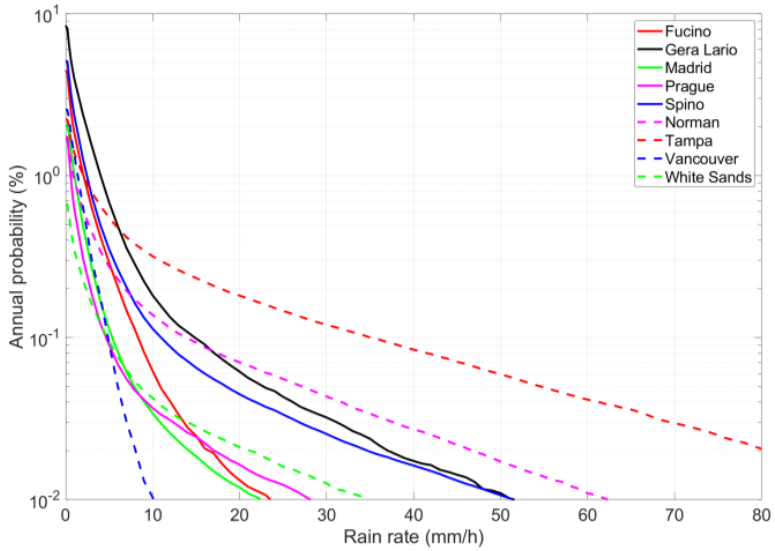

Figure 2. Annual probability distribution (%) $P(R)$ of exceeding the value indicated in abscissa at the indicated sites. Spino d'Adda: continuous blue line; Gera Lario: continuous black line; Fucino: continuous red line; Madrid: continuous green line; Prague: continuous magenta line; Tampa: dashed red line; Norman: dashed magenta line; White Sands: dashed green line; Vancouver: dashed blue line.

Figure 3 shows the average annual probability distribution $P(A)$ of exceeding A (dB) at 80 GHz, circular polarization, calculated with Equation (29) of Reference [4]. The large differences found in Figure 2 are substantially reiterated.

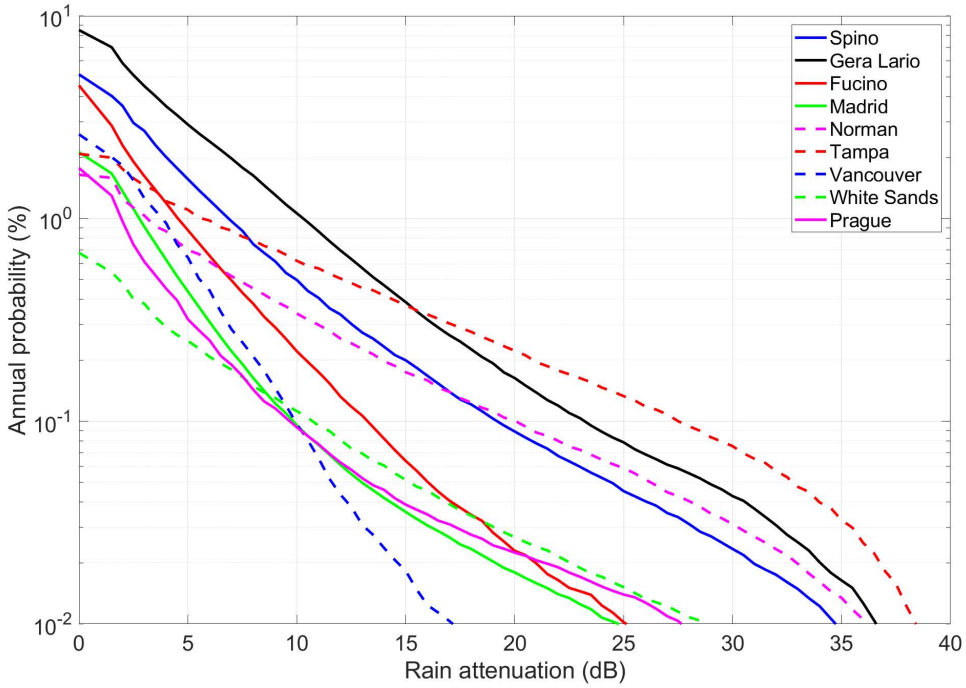

Figure 3. Annual probability distribution (%) $P(A)$ of exceeding the value indicated in abscissa–80 GHz, circular polarization, zenith paths–at the indicated sites. Spino d'Adda: continuous blue line; Gera Lario: continuous black line; Fucino: continuous red line; Madrid: continuous green line; Prague: continuous magenta line; Tampa: dashed red line; Norman: dashed magenta line; White Sands: dashed green line; Vancouver: dashed blue line.

These probability distributions are, of course, the first information asked for by satellite communication designers because they indicate, for a given outage probability $P_{out} = P(A)$, the power margin A necessary to maintain service continuity. For example, in the Spino d'Adda area (such as in Milan, 20 km away), if the rainfall outage probability tolerated by users of the GeoSurf satellite constellations is 0.01% of the time, then the minimum link power margin is 19 dB. In the Tampa area, it is 27 dB.

The fade durations that add up to 0.01% of the time are, of course, made of many intervals whose impact on system design can be studied and assessed just according to $P_{S,A}(D)$ and $P_{S,B}(D)$ of the area; therefore, in the next section, we report these probabilities.

4. Fade Duration Experimental Results

Figures 4 and 5 show $P_{S,A}(D)$ and $P_{S,B}(D)$ for some thresholds in the zenith paths at Spino d'Adda and Tampa. $D \geq 1$ min, the time resolution of $R(t)$ and $A(t)$. For the other sites listed in Table 1, their probability distributions are reported in Appendix A. Notice that the blue line gives $P_{S,A}(D)$ and $P_{S,B}(D)$ for $S = 0$ dB, hence the probability distributions of rainfall intervals of the single rain events (thunderstorms, etc.)

From Figures 4 and 5 and Appendix A, we can observe the following features:

a. As threshold increases, fade duration largely decreases, as physically expected.
b. A fade duration D is exceeded with very different probability at the different sites; or, at the same probability, D is diverse.
c. The probability distributions tend to overlap at the largest thresholds. In other words, the same fade duration is also substantially found at higher thresholds, as shown in Figure 1.

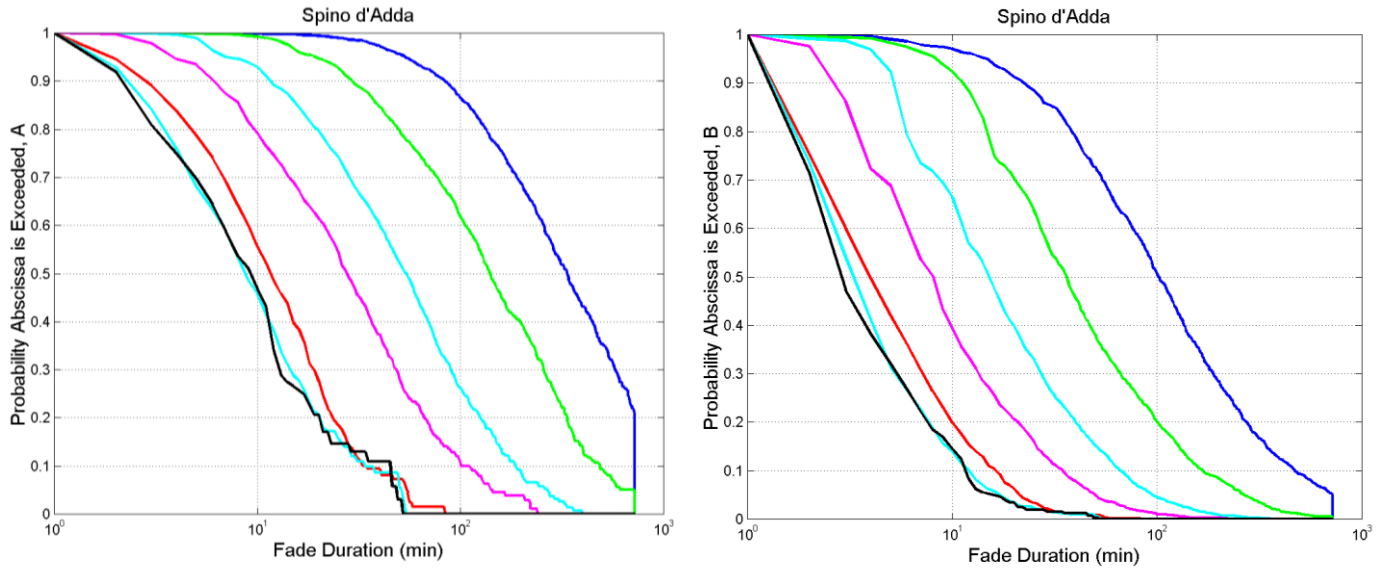

(**a**) (**b**)

Figure 4. Spino d'Adda. (**a**) Probability distribution $P_{S,A}(D)$ of exceeding the value indicated in abscissa at the following thresholds: 0 dB, blue; 3 dB, green; 6 dB, cyan; 10 dB, magenta; 20 dB, red; 29∼ 40 dB, cyan and black; (**b**) $P_{S,B}(D)$, same legend.

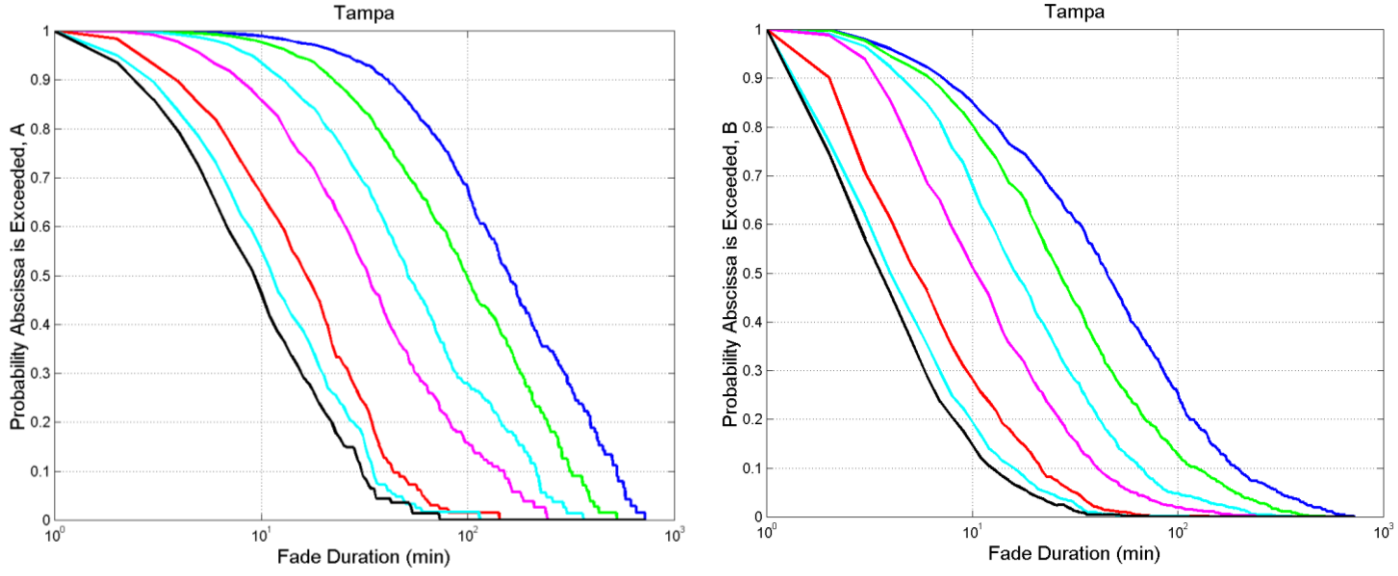

(**a**) (**b**)

Figure 5. Tampa. (**a**) Probability distribution $P_{S,A}(D)$ of exceeding the value indicated in abscissa at the following thresholds: 0 dB, blue; 3 dB, green; 6 dB, cyan; 10 dB, magenta; 20 dB, red; 29∼ 40 dB, cyan and black; (**b**) $P_{S,B}(D)$, same legend.

The two processes are, of course, not independent. Figure 6 shows the median value–value exceeded with probability 0.5—in process B, D_B (min), versus the median value in process A, D_A (min), for the same threshold, and all sites. Recall that the median value is a statistical parameter more useful than the mean value when a stochastic variable varies in a large range, as fade duration does. We can see that $D_B < D_A$, always.

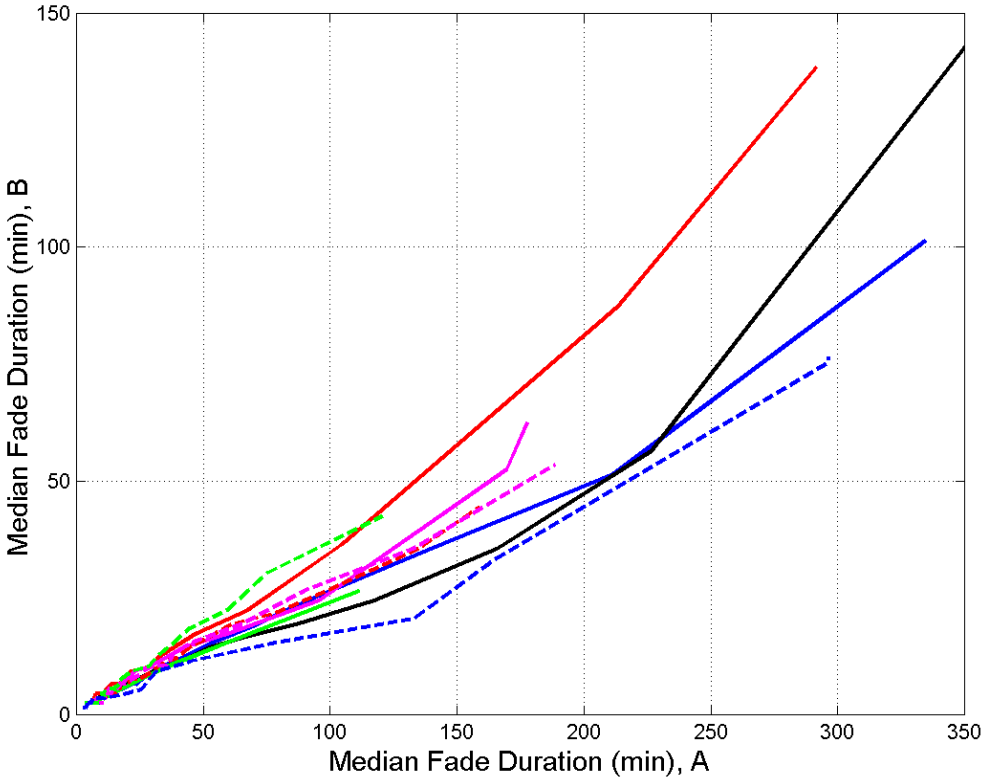

Figure 6. Median fade duration in process B (y-axis) versus the median fade duration in process A (x-axis) at the indicated sites. Spino d'Adda: continuous blue line; Gera Lario: continuous black line; Fucino: continuous red line; Madrid: continuous green line; Prague: continuous magenta line; Tampa: dashed red line; Norman: dashed magenta line; White Sands: dashed green line; Vancouver: dashed blue line.

Remember that D_B refers to the number of occurrences and D_A to the fraction of time. For example, in Spino d'Adda, we find that when $D_A = 100$ min then $D_B = 25$ min; therefore, at a particular threshold (it is $S \approx 3$ dB, Figure 4a, green line), 50% of the outages are due to fade durations longer than 25 min, while 50% of the outage time is due to fade durations longer than 100 min, events that occur with probability 0.2 (Figure 4b, green line).

As observed above, sites belong to quite different climatic regions, and this is clearly observable in Figures 1–6 and Appendix A. Now, it is interesting to see how many occurrences are found in the sites.

Figure 7 shows the average annual number of outage occurrences versus attenuation threshold. It is interesting to notice that peak values can be quite sharp, mostly below 10 dB, especially in Gera Lario. Tampa, Norman and White Sands show less pronounced peaks. These features are not directly obtainable from the $P(A)'s$ shown in Figure 3, but only from the histograms giving $P_{S,A}(D)$ and $P_{S,B}(D)$.

Notice the quite different behavior of Gera Lario, very likely due to the particular geographical location among high mountains at the Northern Lake Como, with more frequent rain events than at Spino d'Adda, just 84 km away.

Also of interest is the cumulative number of occurrences versus threshold S at equal fade duration exceeded, i.e., the actual cumulative number of occurrences which yield $P_{S,B}(\tau \leq D)$. Figure 8 shows these curves, in 5 min steps, for Spino d'Adda and Tampa, while Appendix B reports the data of the other sites.

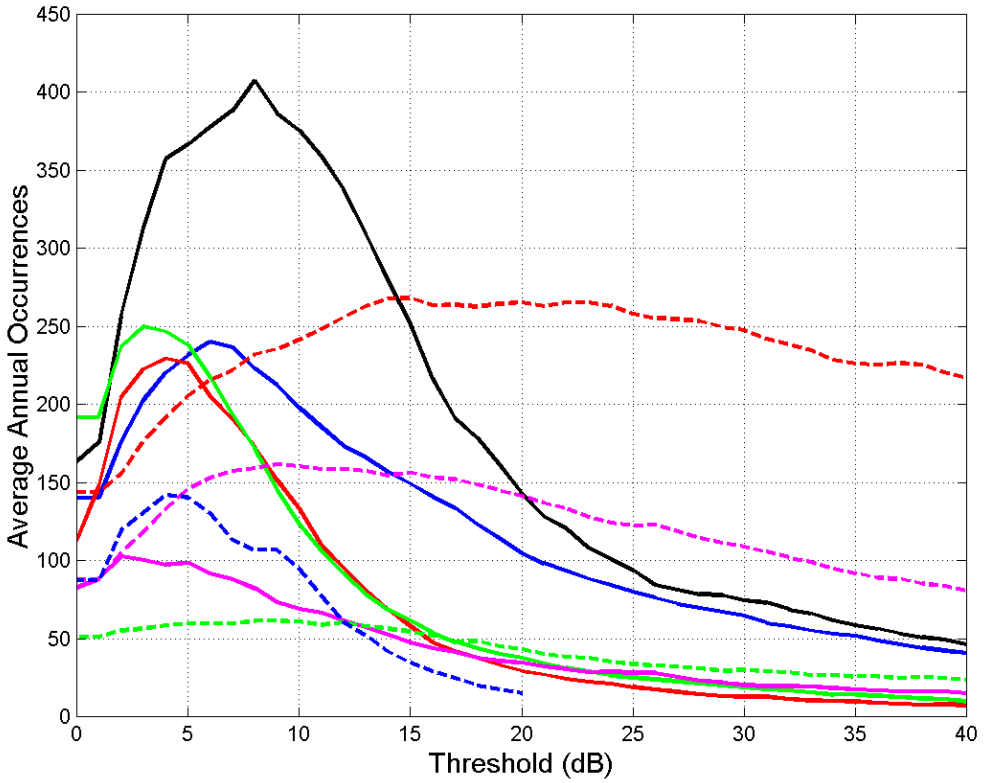

Figure 7. Average annual number of outage occurrences at the threshold indicated in abscissa—80 GHz, circular polarization, zenith paths–at the indicated sites. Spino d'Adda: continuous blue line; Gera Lario: continuous black line; Fucino: continuous red line; Madrid: continuous green line; Prague: continuous magenta line; Tampa: dashed red line; Norman: dashed magenta line; White Sands: dashed green line; Vancouver: dashed blue line.

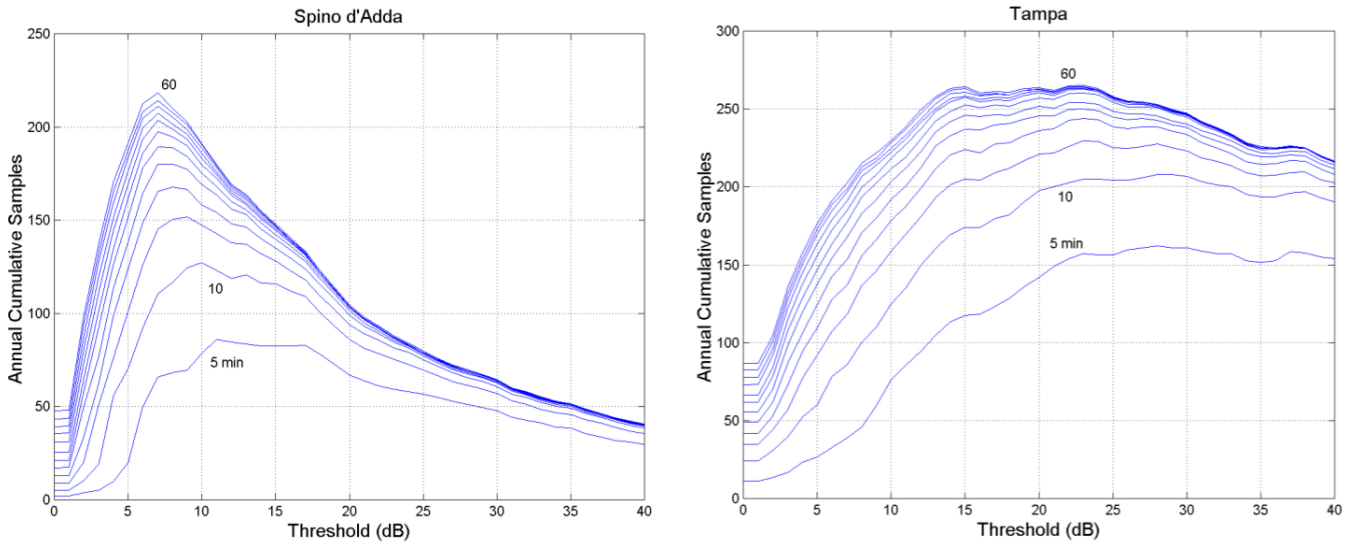

(**a**) (**b**)

Figure 8. Annual cumulative number of outage occurrences at the threshold indicated in abscissa, 80 GHz, circular polarization, zenith paths at: (**a**) Spino d'Adda; (**b**) Tampa. The continuous lines are drawn at equal fade duration, in 5 min steps from $\tau = 5$ min to $\tau = 60$. The y–axis has different range.

From Figure 8 and Appendix B, we can observe the following features:

(a) As threshold increases, the occurrences largely decrease for any D, as physically expected.
(b) As fade duration D increases, sharp peaks are clearly evident in many sites.
(c) Peaks tend to occur at lower thresholds.
(d) As fade duration D increases, curves tend to collapse, in agreement with the probability distributions $P_{S,B}(D)$ shown in Figure 4a and b. For example, the curves regarding $D = 50 \sim 60$ min tend to coincide.

As we have previously recalled, the two processes are not independent and this fact can be assessed by studying $P_{S,B}(D)$ versus $P_{S,A}(D)$, as we show in the next section by defining a useful parameter, the uniformity index.

5. Processes A and B Interdependence

To show that the two processes are not independent, let us study the relationship between $P_{S,B}(D)$ and $P_{S,A}(D)$, at equal D, i.e., the function $P_{S,B}(D) = f(P_{S,A}(D))$. Figure 9a shows this relationship for Spino d'Adda. Each curved black line refers to a threshold, from 0 to 40 dB (41 curves). Similar curves are found for all the other sites (Appendix C). Notice that the D scale is reversed in both x- and y- axes shown in Figure 9; in other words, D decreases as $P_{S,B}(D)$ and $P_{S,A}(D)$ increase.

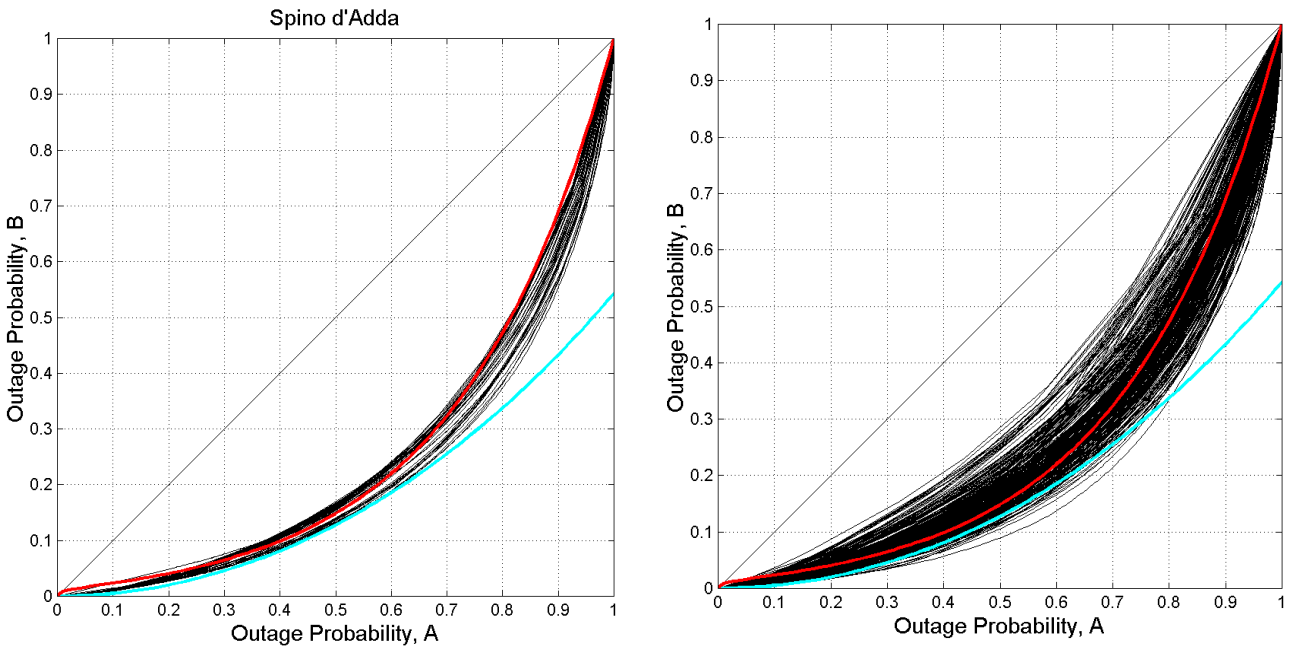

(**a**) (**b**)

Figure 9. $P_{S,B}(D)$ (y-axis) versus $P_{S,A}(D)$ x-axis, for thresholds from 0 to 40 dB, 80 GHz. The continuous red line is drawn from Equation (3); the continuous cyan line is drawn from Equation (5). (**a**) Spino d'Adda; (**b**) All sites.

These curves give the following information. Since the largest values of D exceeded give $P_{S,B}(D) \approx P_{S,A}(D) \approx 0$, we can see that a large increase in $P_{S,A}(D)$ does not correspond to a similar increase in $P_{S,B}(D)$. In other words, few samples of the longest fades give a significant fraction of time but not a significant number of occurrences. For example, if $P_{S,A}(D) \approx 0.4$ then $P_{S,B}(D) \approx 0.1$.

The approximate exponential nature of the relationships shown in Figure 9a can be modelled by the following equation, with $x = P_{S,A}(D)$, $y = P_{S,B}(D)$:

$$y(x) = e^{\beta x}(1 - e^{-x})^{\alpha}/k \quad (3)$$

$$k = e^{\beta}(1 - e^{-1})^{\alpha} \tag{4}$$

In Equations (3) and (4), $\alpha = 3.5385$, $\beta = 0.2958$ and the corresponding curve is the red line drawn in Figure 9. These numerical values have been determined by averaging the log values of α and β of Equation (3) obtained by a best–fit analysis of each of the 41 curves. Notice that Equation (3) tends to represent an average value at small x and an upper bound at large x.

The cyan line drawn in Figure 9 is the hyperbolic cosine minus 1:

$$y_C = \cosh(x) - 1 \tag{5}$$

Equation (5) practically gives a lower bound for all sites (Appendix C), quite precise in the range $x = 0 \sim 0.7$. For $x = 0.7$ $y_C = 0.2552$.

Figure 9b shows the curves of all sites and thresholds. We can see that Equation (3), with the values of α and β found for Spino d'Adda, is a good estimate of the average value. In conclusion, Equations (3) and (4) describe useful overall relationships that link $P_{S,B}(D)$ to $P_{S,A}(D)$.

The 45° line drawn in Figure 9 represents the curve linking $P_{S,B}(D)$ and $P_{S,A}(D)$ in the unrealistic case in which all fade durations were equal, namely when the two processes coincide. It is, however, a good reference line, as we show now by defining a uniformity index U in the next section.

6. Uniformity Index

How can we measure the difference between real cases–fade durations fragmented in many different intervals with changing threshold and site–and the limiting case of identity/uniformity of the two processes when all fades last the same time? We propose the following index $U(S)$, referred to as the uniformity index and a function of threshold S, defined by:

$$U(S) = \frac{\int_0^1 P_{S,B}(D) d(P_{S,A}(D))}{0.5} \tag{6}$$

In other words, Equation (6) is the ratio between the area under each function $P_{S,B}(D) = f(P_{S,A}(D))$ shown in Figure 9 and in Appendix C, and the area under the 45° line, which is 0.5. Therefore $0 < U \leq 1$.

Figure 10 shows uniformity index versus threshold, for each site. We can observe the following features:

(a) $U(S) > \sim 0.4$ for all sites.
(b) For $S = 0$ dB, $U(0)$ ranges from $\sim$ 0.42 to $\sim$ 0.58. Since this value refers to the single rain events (i.e., the time series $R(t)$ of each rain event), then the duration of rain events does change in a large range. In fact, if all rain events were of equal duration D, they would give $P_{S,B}(D) = P_{S,A}(D) = \delta(1)$, $U(0) = 1$. This case would be represented by the point (1,1) in Figure 9, with probability $\delta(1)$, a Dirac impulse of unit area.
(c) Some sites show marked dips at low thresholds. In other words, at these thresholds the two processes are the furthest away from the uniformity model (Spino d'Adda, Gera Lario, Madrid, Vancouver).
(d) As the threshold increases, $U(S)$ increases; therefore, the two processes tend to be closer to the uniformity model at larger rain attenuation. This is a sound physical result because fades tend to be more similar in duration at large rain attenuation (see, for example, Figure 1). $U(S)$ approaches 1 at very large thresholds (Madrid, Vancouver).
(e) The red line, Equation (3), gives $U = 0.2605/0.5 = 0.521$ (a line $y = 0.521$ in Figure 10) practically the mid–range value at $S = 0$ dB: $0.42 + 0.58)/2 = 0.5$.

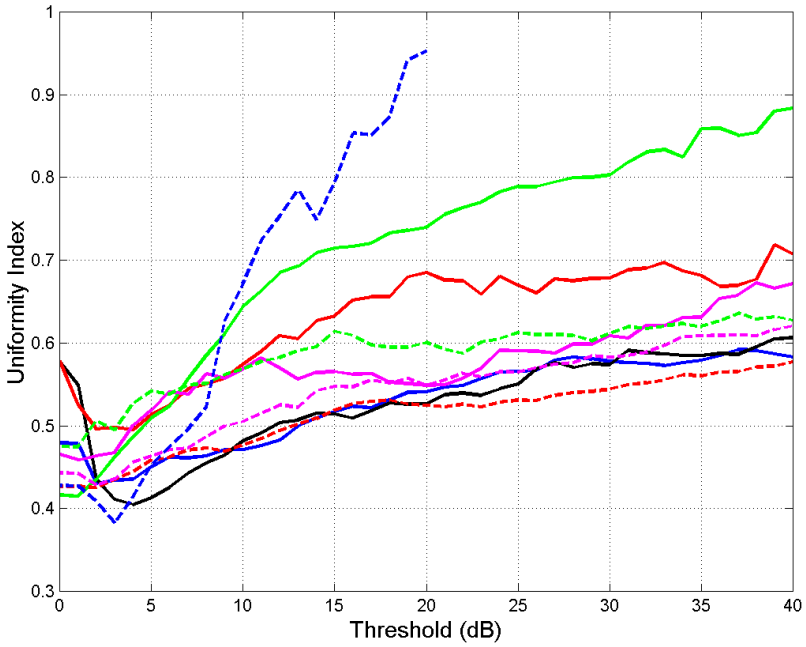

Figure 10. Uniformity index versus the threshold indicated in abscissa at the indicated sites. Spino d'Adda: continuous blue line; Gera Lario: continuous black line; Fucino: continuous red line; Madrid: continuous green line; Prague: continuous magenta line; Tampa: dashed red line; Norman: dashed magenta line; White Sands: dashed green line; Vancouver: dashed blue line.

7. Conclusions

Fade duration is the second most important link parameter required for designing a satellite link faded by rain because it gives the interval the rain attenuation time series $A(t)$ exceeds an attenuation threshold S (dB), namely the link power margin compared to clear sky. Since no measurements are available for zenith paths of GeoSurf satellite constellations, we have simulated $A(t)$ with the Synthetic Storm Technique at sites located in different climatic regions.

We have studied the two stochastic processes of fade durations, A and B. Process B gives the statistics of outages, and process A gives the statistics of outage duration. We have found that fade duration D largely decreases as threshold increases, and it is exceeded with different probability at the diverse sites of Table 1.

To show that the two processes are not independent, we have studied the relationship between their probabilities and defined a uniformity index $U(S)$, which compares real cases—fade durations fragmented in many different intervals with changing threshold and site—with the limiting case of all fades lasting the same time. We have found that $U(S) >\sim 0.4$ for all sites. As the threshold increases, $U(S)$ increases; therefore, the two processes tend to be closer to the uniformity model at larger rain attenuation. $U(S)$ approaches 1 at very large thresholds.

These results should guide the designers of future GeoSurf satellite constellations to take care of the diverse communications services, differently affected by the two fade duration processes. Process B (occurrences) impacts, especially, on non–real-time services, such as data delivery, which can be more disturbed by the number of outages rather than by their duration. Process A (fraction of time) impacts, especially on real–time services such as television, video conference etc., which are more disturbed by the duration of the outage.

Author Contributions: Conceptualization, E.M. and C.R.; methodology; software, E.M. and C.R.; validation, E.M. and C.R.; investigation, E.M. and C.R.; data curation, E.M. and C.R.; writing—original draft preparation, E.M.; writing—review and editing, E.M. and C.R.; visualization, E.M. and C.R. All authors have read and agreed to the published version of the manuscript.

Funding: This research received no external funding.

Institutional Review Board Statement: Not applicable.

Data Availability Statement: Data available from the authors.

Conflicts of Interest: The authors declare no conflicts of interest.

Appendix A

In this appendix, we report the probability distribution $P_{S,A}(D)$ and $P_{S,B}(D)$ of exceeding D for some thresholds for the sites listed in Table 1.

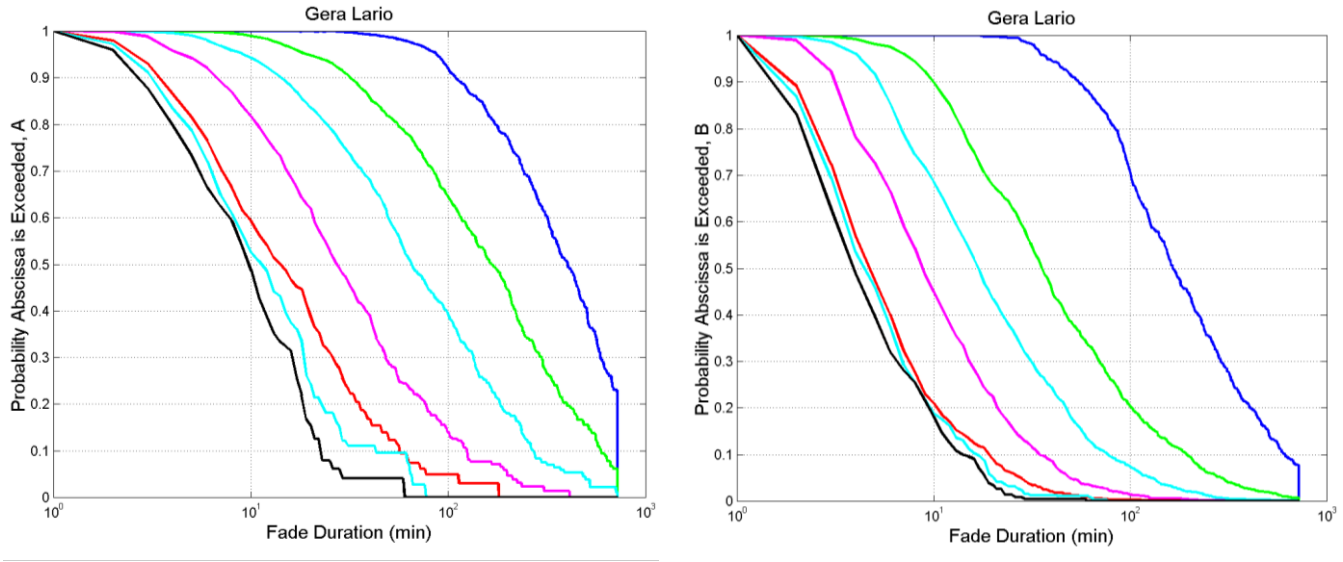

(**a**) (**b**)

Figure A1. Gera Lario. (**a**) Probability distribution $P_{S,A}(D)$ of exceeding the value indicated in abscissa at the following thresholds: 0 dB, blue; 3 dB, green; 6 dB, cyan; 10 dB, magenta; 20 dB, red; 29∼ 40 dB, cyan and black; (**b**) $P_{S,B}(D)$, same legend.

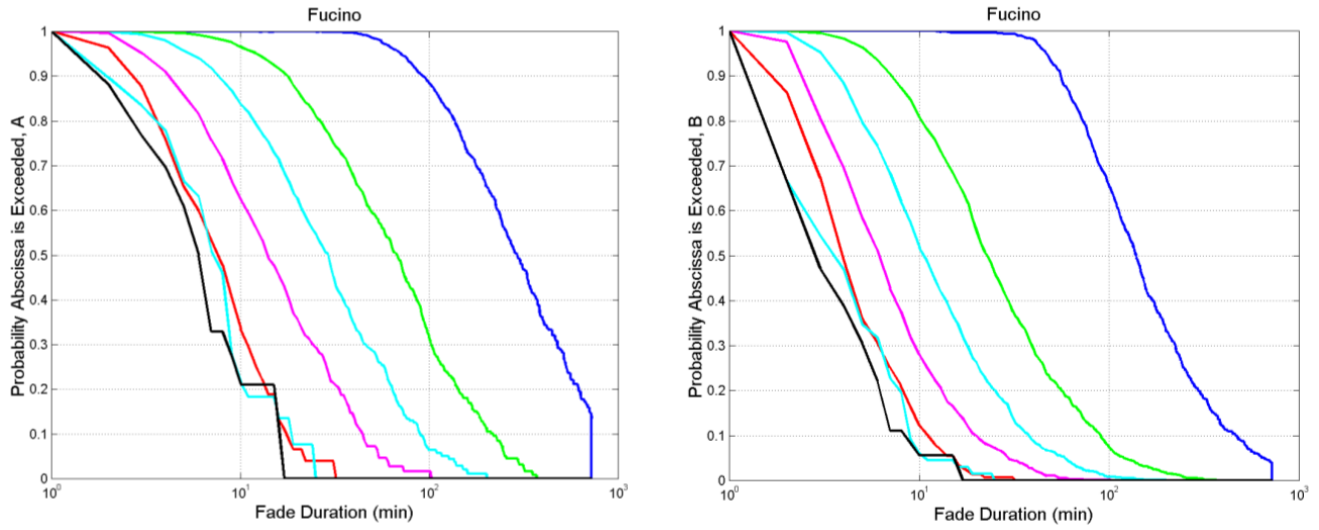

(**a**) (**b**)

Figure A2. Fucino. (**a**) Probability distribution $P_{S,A}(D)$ of exceeding the value indicated in abscissa at the following thresholds: 0 dB, blue; 3 dB, green; 6 dB, cyan; 10 dB, magenta; 20 dB, red; 29∼ 40 dB, cyan and black; (**b**) $P_{S,B}(D)$, same legend.

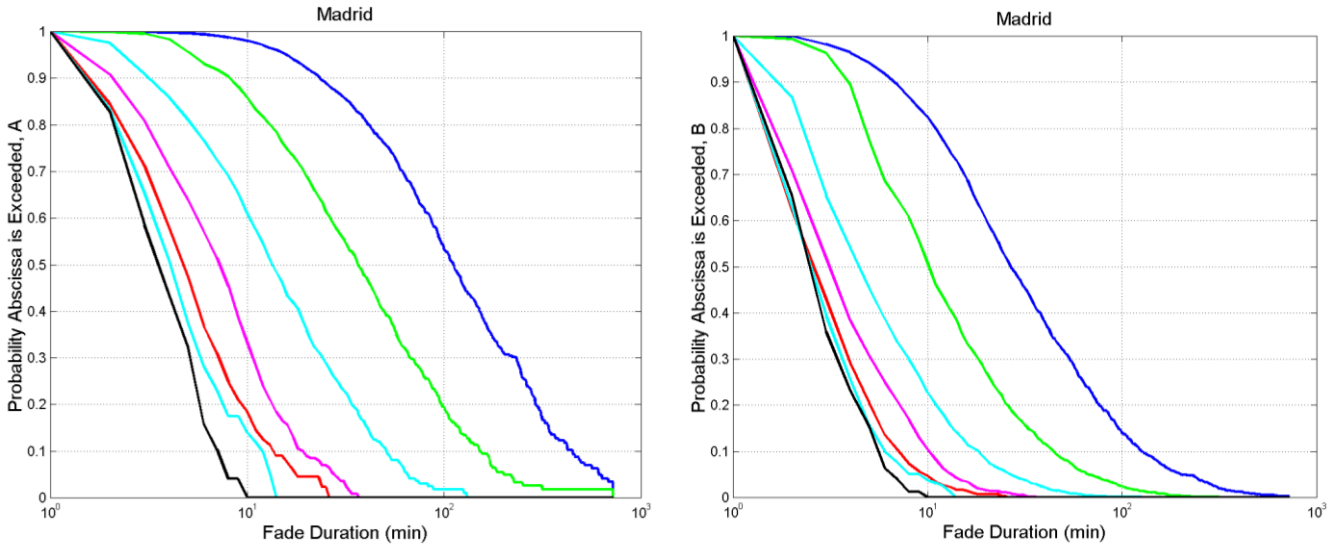

(**a**) (**b**)

Figure A3. Madrid. (**a**) Probability distribution $P_{S,A}(D)$ of exceeding the value indicated in abscissa at the following thresholds: 0 dB, blue; 3 dB, green; 6 dB, cyan; 10 dB, magenta; 20 dB, red; 29∼ 40 dB, cyan and black; (**b**) $P_{S,B}(D)$, same legend.

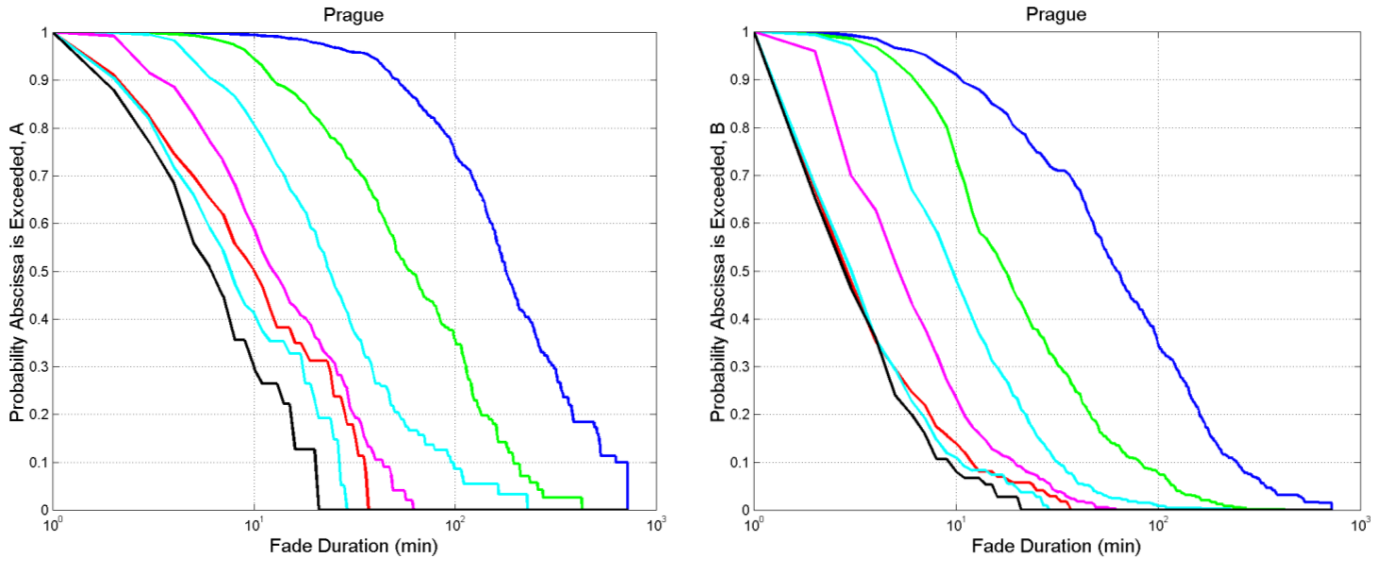

(**a**) (**b**)

Figure A4. Prague. (**a**) Probability distribution $P_{S,A}(D)$ of exceeding the value indicated in abscissa at the following thresholds: 0 dB, blue; 3 dB, green; 6 dB, cyan; 10 dB, magenta; 20 dB, red; 29∼ 40 dB, cyan and black; (**b**) $P_{S,B}(D)$, same legend.

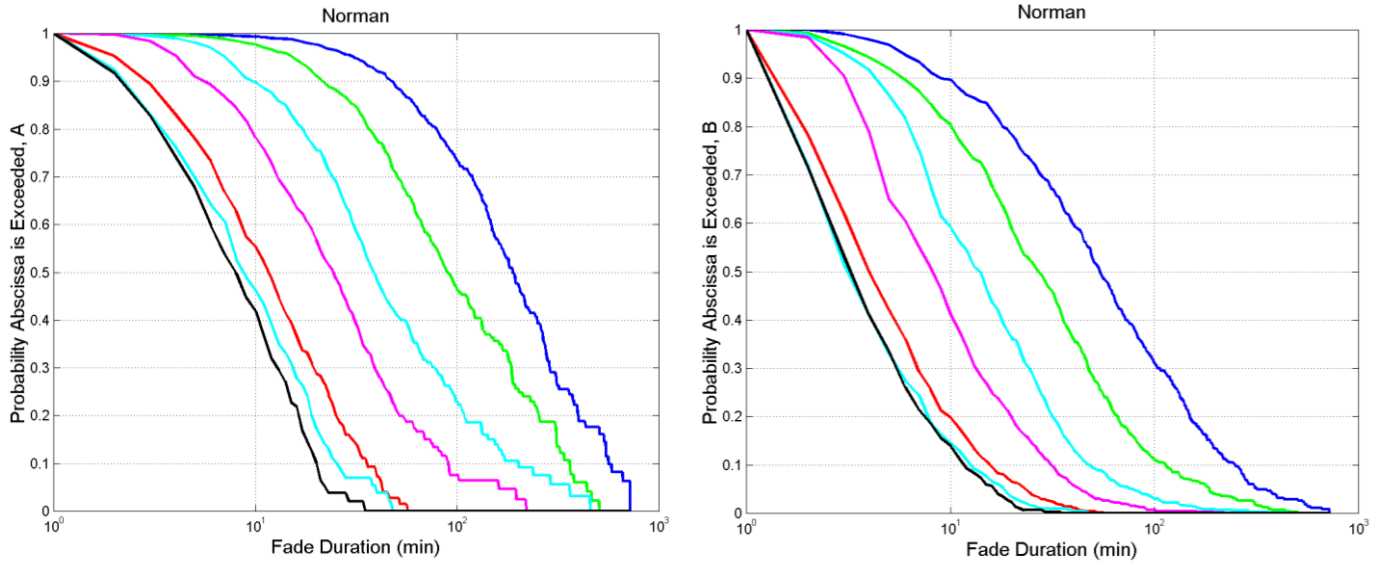

(**a**) (**b**)

Figure A5. Norman. (**a**) Probability distribution $P_{S,A}(D)$ of exceeding the value indicated in abscissa at the following thresholds: 0 dB, blue; 3 dB, green; 6 dB, cyan; 10 dB, magenta; 20 dB, red; 29∼ 40 dB, cyan and black; (**b**) $P_{S,B}(D)$, same legend.

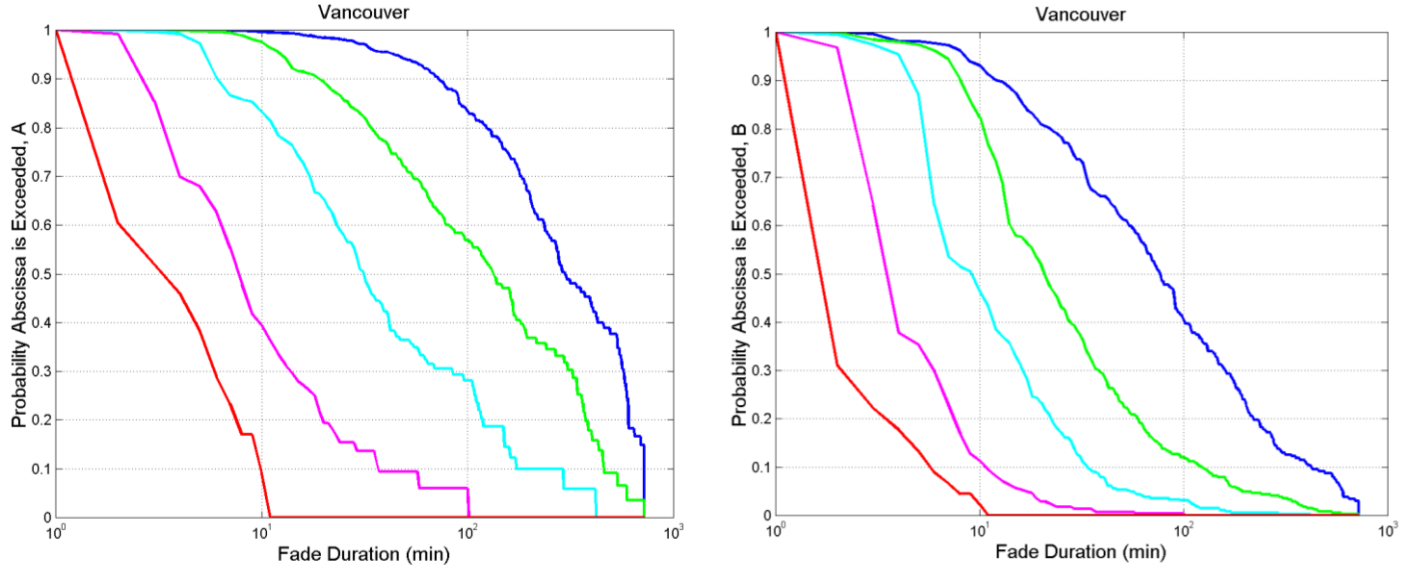

(**a**) (**b**)

Figure A6. Vancouver. (**a**) Probability distribution $P_{S,A}(D)$ of exceeding the value indicated in abscissa at the following thresholds: 0 dB, blue; 3 dB, green; 6 dB, cyan; 10 dB, magenta; 20 dB, red; 29∼ 40 dB, cyan and black; (**b**) $P_{S,B}(D)$, same legend.

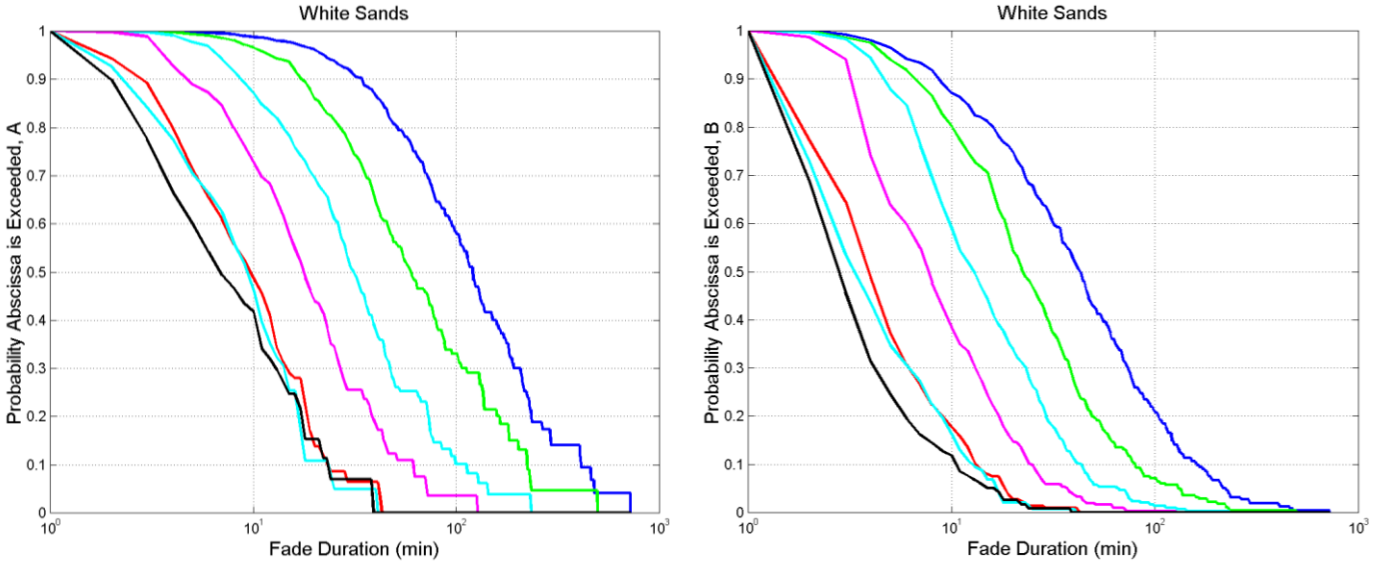

(**a**) (**b**)

Figure A7. White Sands. (**a**) Probability distribution $P_{S,A}(D)$ of exceeding the value indicated in abscissa at the following thresholds: 0 dB, blue; 3 dB, green; 6 dB, cyan; 10 dB, magenta; 20 dB, red; 29∼ 40 dB, cyan and black; (**b**) $P_{S,B}(D)$, same legend.

Appendix B

In this appendix, we report the annual cumulative number of outage occurrences for some thresholds and sites listed in Table 1.

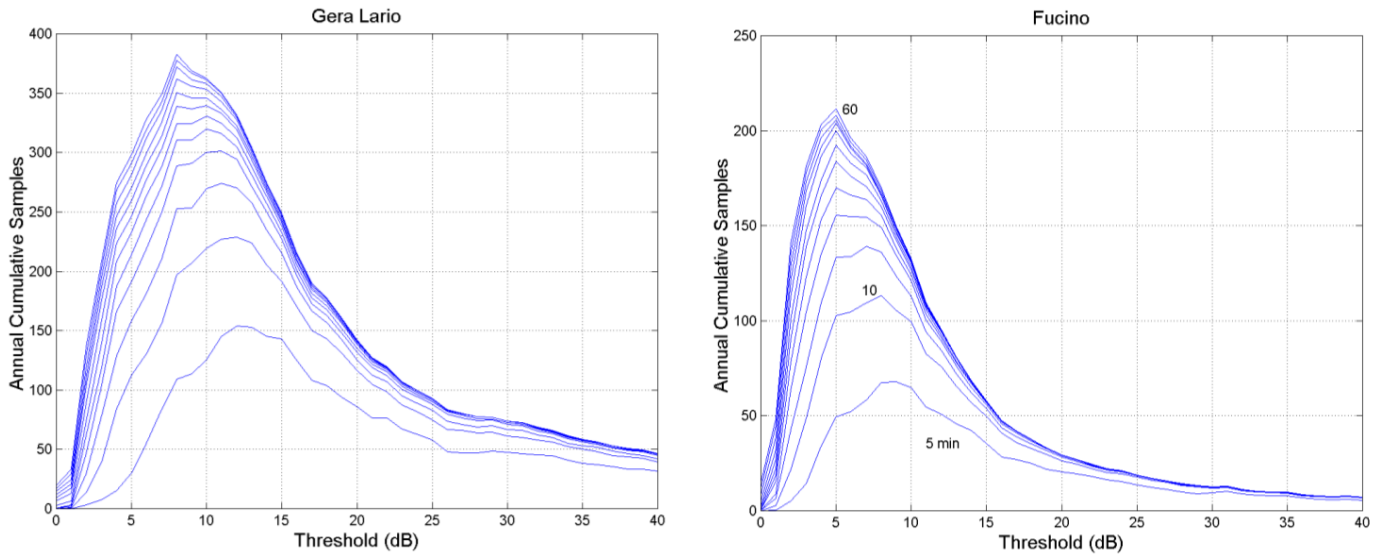

(**a**) (**b**)

Figure A8. Annual cumulative number of outage occurrences at the threshold indicated in abscissa, 80 GHz, circular polarization, zenith paths: (**a**) Gera Lario; (**b**) Fucino. The lines refer to constant fade duration, in 5 min steps, from $\tau = 5$ min to $\tau = 60$. The y-axis has different range.

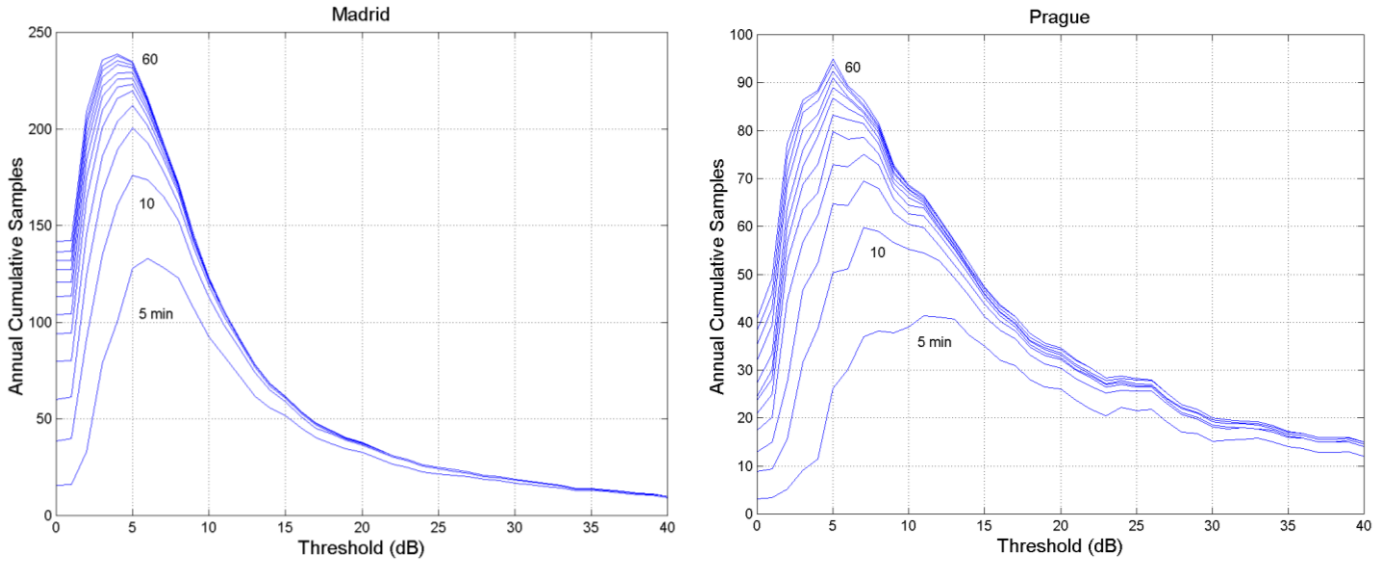

(**a**) (**b**)

Figure A9. Annual cumulative number of outage occurrences at the threshold indicated in abscissa, 80 GHz, circular polarization, zenith paths: (**a**) Madrid; (**b**) Prague. The lines refer to constant fade duration, in 5 min steps, from $\tau = 5$ min to $\tau = 60$. The y-axis has different range.

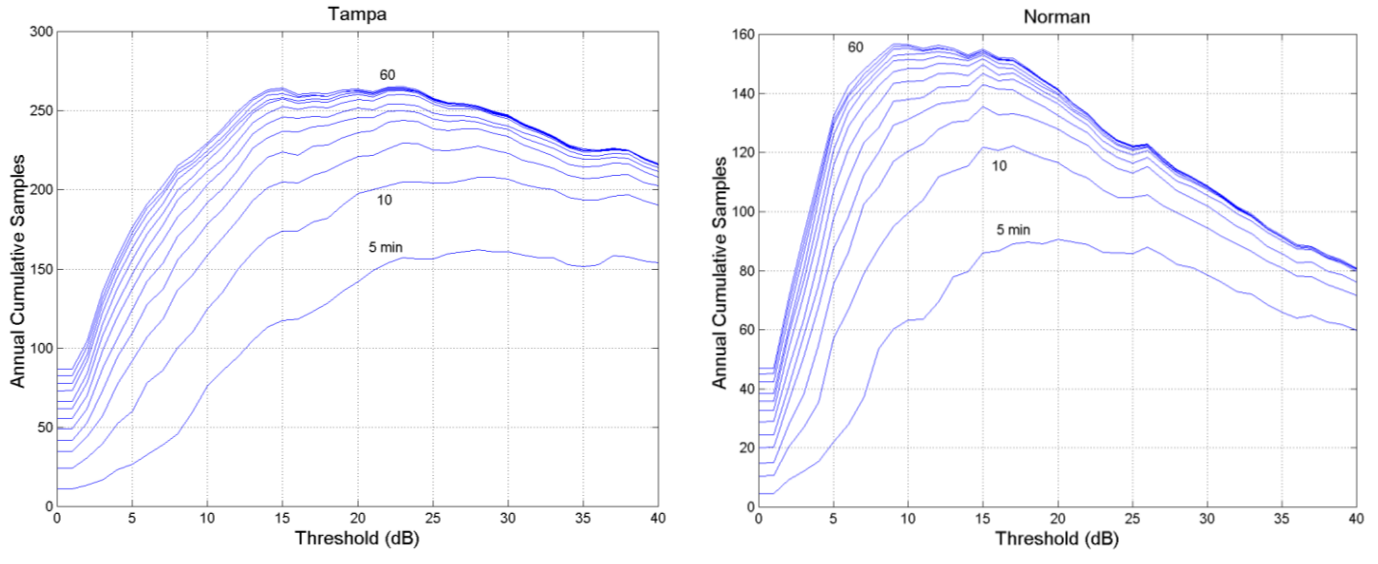

(**a**) (**b**)

Figure A10. Annual cumulative number of outage occurrences at the threshold indicated in abscissa, 80 GHz, circular polarization, zenith paths: (**a**) Tampa; (**b**) Norman. The lines refer to constant fade duration, in 5 min steps, from $\tau = 5$ min to $\tau = 60$. The y-axis has different range.

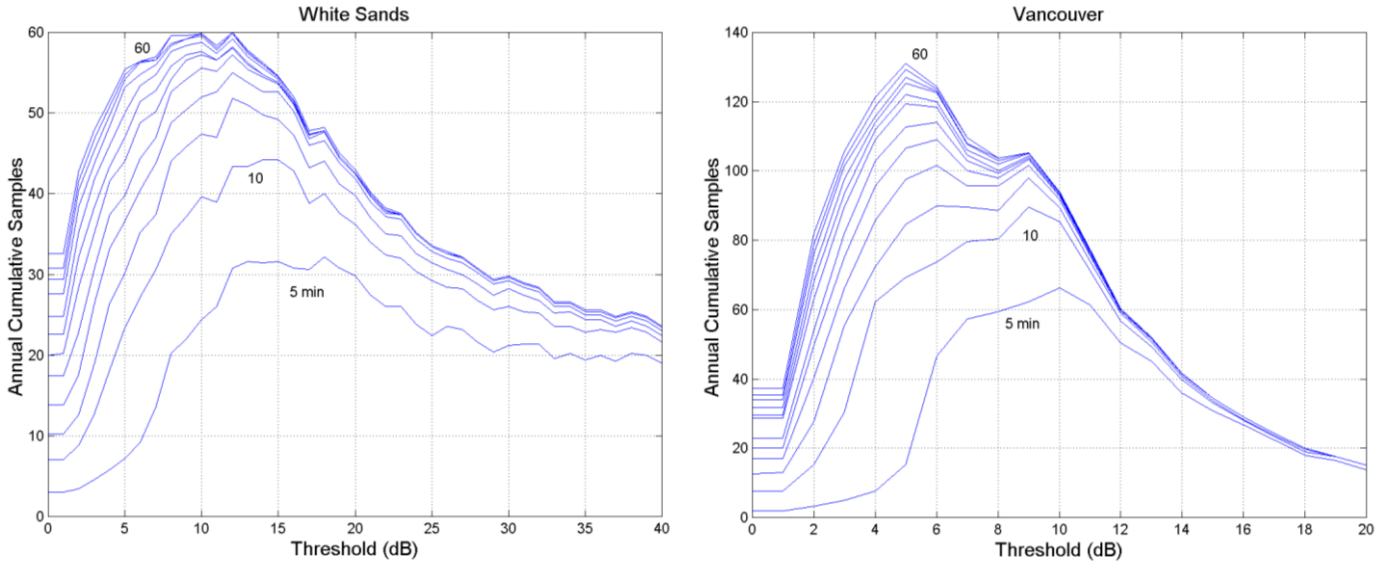

(**a**) (**b**)

Figure A11. Annual cumulative number of outage occurrences at the threshold indicated in abscissa, 80 GHz, circular polarization, zenith paths: (**a**) White Sands; (**b**) Vancouver. The lines refer to constant fade duration, in 5 min steps, from $\tau = 5$ min to $\tau = 60$. The y-axis has different range.

Appendix C

In this appendix, we report $P_{S,B}(D)$ (y–axis) versus $P_{S,B}(D)$ x–axis for thresholds from 0 to 40 dB, for the sites listed in Table 1.

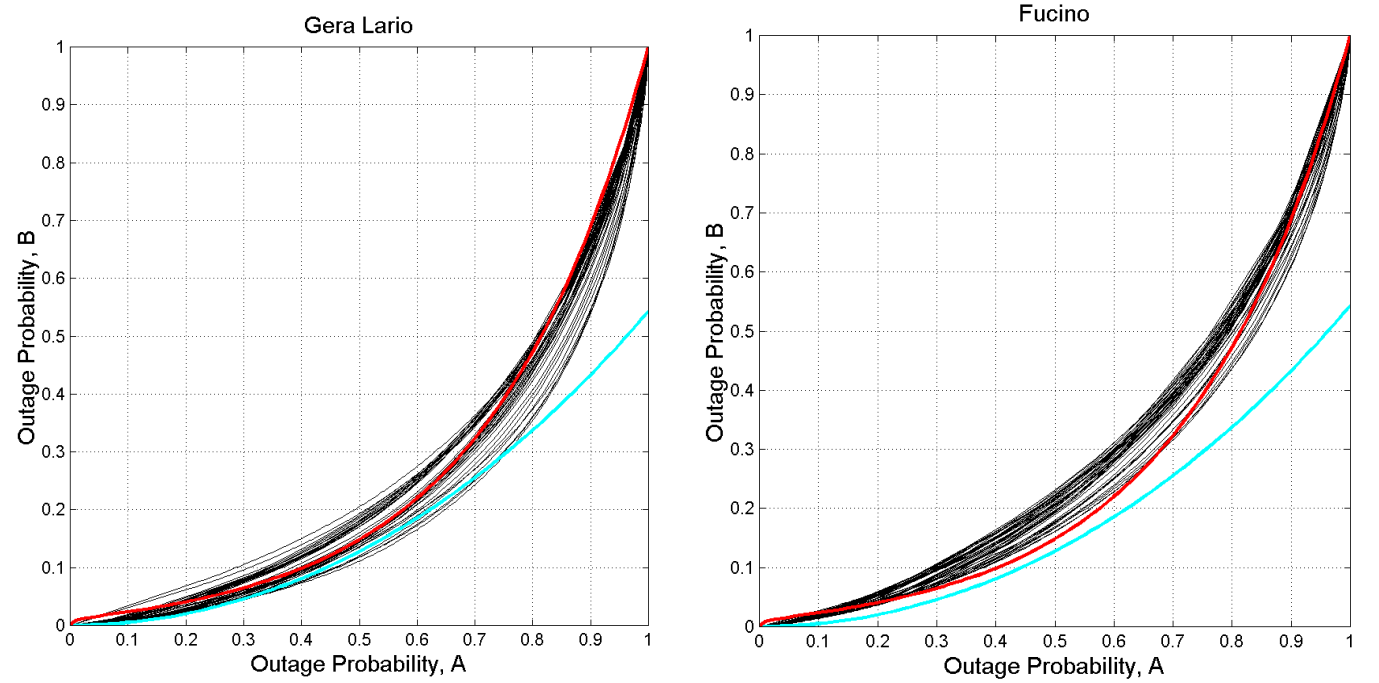

(**a**) (**b**)

Figure A12. $P_{S,B}(D)$ (y-axis) versus $P_{S,A}(D)$ x-axis, for thresholds from 0 to 40 dB, 80 GHz, circular polarization, zenith paths: (**a**) Gera Lario; (**b**) Fucino. The red line is drawn from Equation (3); the cyan line is drawn from Equation (5).

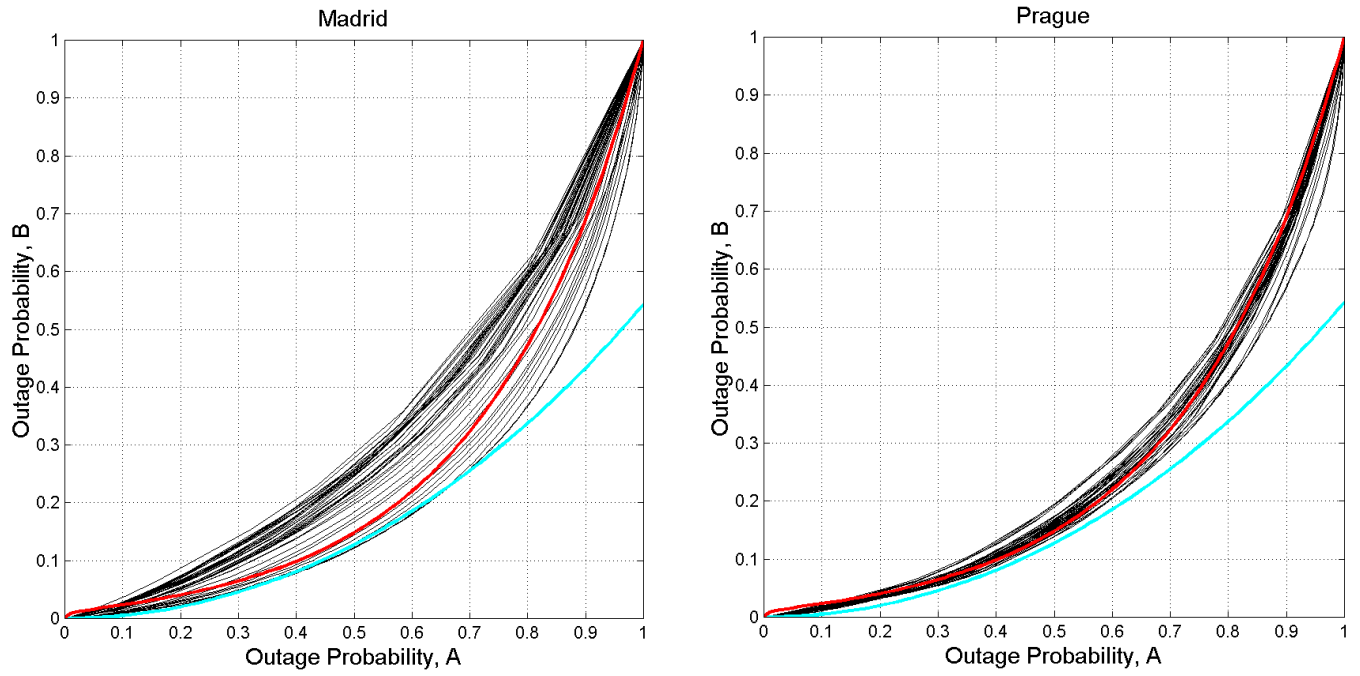

(**a**) (**b**)

Figure A13. $P_{S,B}(D)$ (y-axis) versus $P_{S,A}(D)$ x-axis, for thresholds from 0 to 40 dB, 80 GHz, circular polarization, zenith paths: (**a**) Madrid; (**b**) Prague. The red line is drawn from Equation (3); the cyan line is drawn from Equation (5).

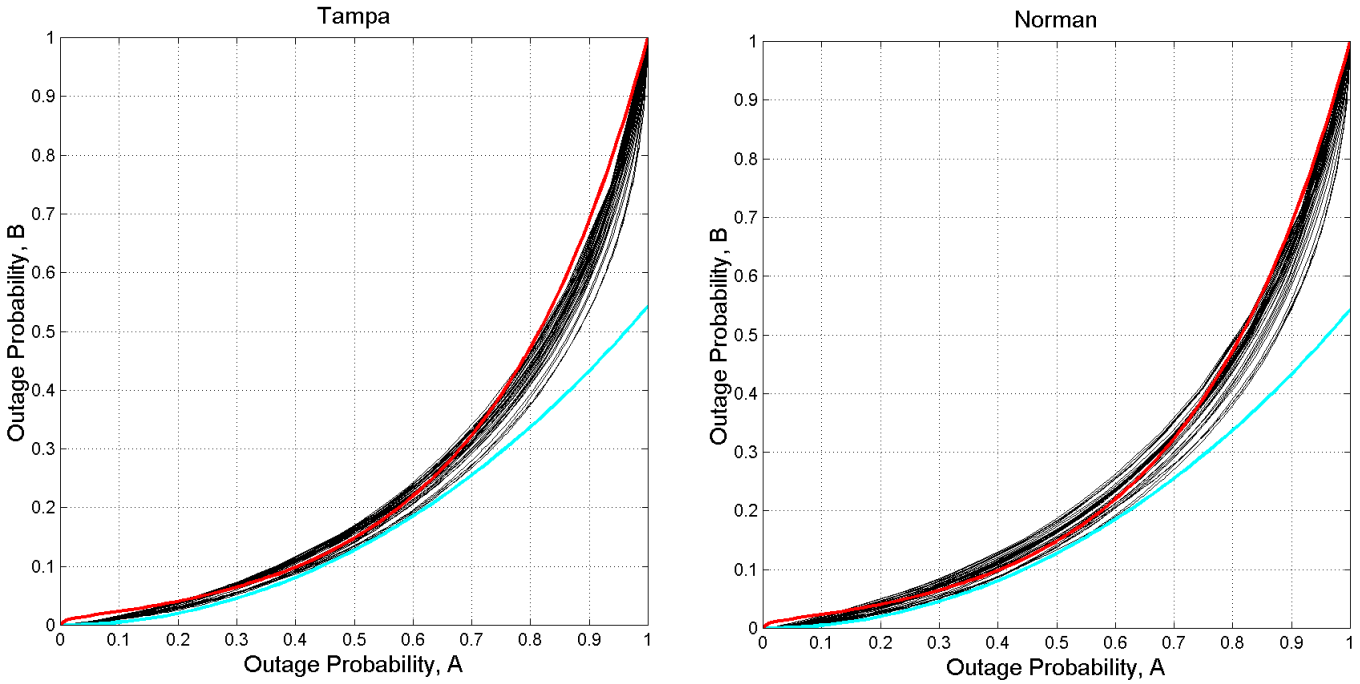

(**a**) (**b**)

Figure A14. $P_{S,B}(D)$ (y-axis) versus $P_{S,A}(D)$ x-axis, for thresholds from 0 to 40 dB, 80 GHz, circular polarization, zenith paths: (**a**) Tampa; (**b**) Norman. The red line is drawn from Equation (3); the cyan line is drawn from Equation (5).

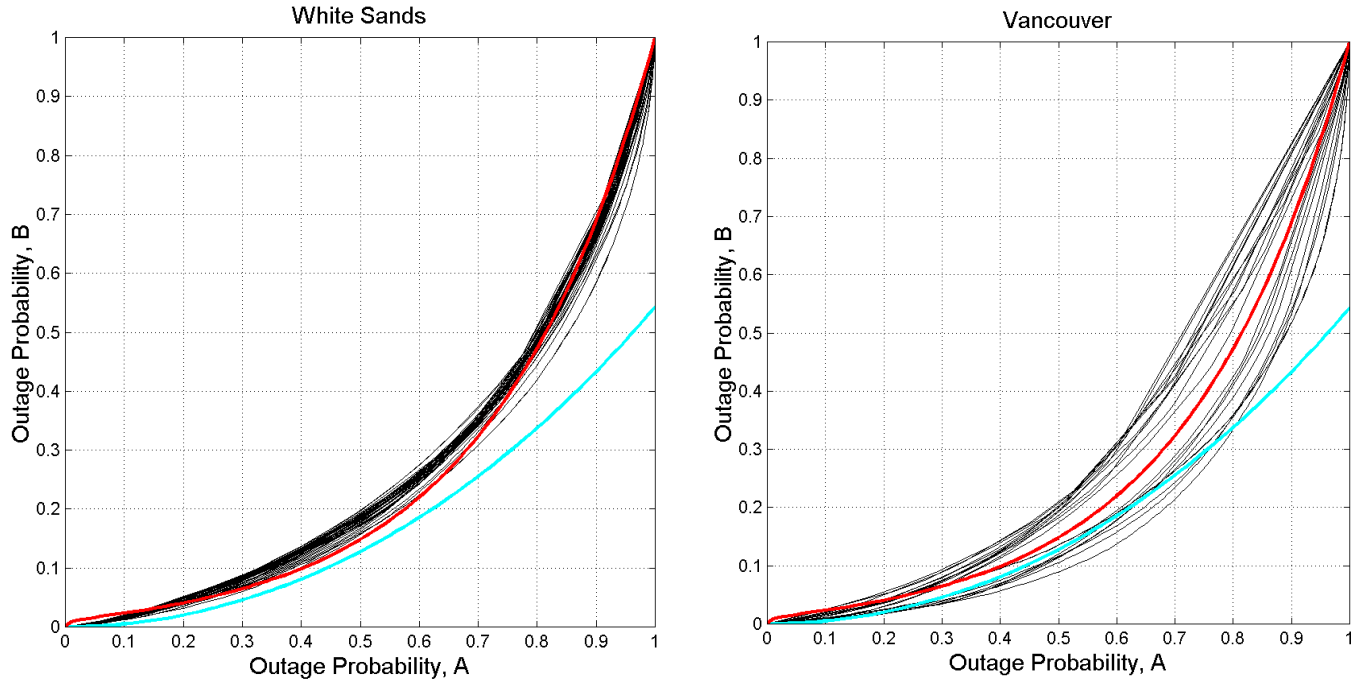

(**a**) (**b**)

Figure A15. $P_{S,B}(D)$ (y-axis) versus $P_{S,A}(D)$ x-axis, 80 GHz, circular polarization, zenith paths: (**a**) White Sands, for thresholds from 0 to 40 dB; (**b**) Vancouver, for thresholds from 0 to 20 dB. The red line is drawn from Equation (3); the cyan line is drawn from Equation (5).

References

1. Matricciani, E. Geocentric Spherical Surfaces Emulating the Geostationary Orbit at Any Latitude with Zenith Links. *Future Internet* **2020**, *12*, 16. [CrossRef]
2. Matricciani, E.; Riva, C.; Luini, L. Tropospheric Attenuation in GeoSurf Satellite Constellations. *Remote Sens.* **2021**, *13*, 5180. [CrossRef]
3. Matricciani, E.; Riva, C. Outage Probability versus Carrier Frequency in GeoSurf Satellite Constellations with Radio–Links Faded by Rain. *Telecom* **2022**, *3*, 504–513. [CrossRef]
4. Matricciani, E. Physical–mathematical model of the dynamics of rain attenuation based on rain rate time series and a two–layer vertical structure of precipitation. *Radio Sci.* **1996**, *31*, 281–295. [CrossRef]
5. Matricciani, E.; Riva, C. Transfer–functions and Linear Distortions in Ultra–Wideband Channels Faded by Rain in GeoSurf Satellite Constellations. *Future Internet* **2023**, *15*, 27. [CrossRef]
6. Turin, G.L. Introduction to spread spectrum antimultipath techniques and their application to urban digital radio. *Proc. IEEE* **1980**, *68*, 328–353. [CrossRef]
7. Pickholtz, R.; Schilling, D.; Milstein, L. Theory of spread–spectrum communications—A tutorial. *IEEE Trans. Commun.* **1982**, *30*, 855–884. [CrossRef]
8. Viterbi, A.J. *CDMA Principles of Spread Spectrum Communications*; Addinson–Wesly: Reading, MA, USA, 1995.
9. Dinan, E.H.; Jabbari, B. Spreading codes for direct sequence CDMA and wideband CDMA celluar networks. *IEEE Commun. Mag.* **1998**, *36*, 48–54. [CrossRef]
10. Veeravalli, V.V.; Mantravadi, A. The coding–spreading trade–off in CDMA systems. *IEEE Trans. Sel. Areas Commun.* **2002**, *20*, 396–408. [CrossRef]
11. Matricciani, E.; Magarini, M.; Riva, C. Feasibility of Ultra–Wideband Channels at Millimeter Wavelengths Faded by Rain in GeoSurf Satellite Constellations. *Telecom* **2023**, *4*, 732–745. [CrossRef]
12. Kelmendi, A.; Hrovat, A.; Mohorčič, M.; Vilhar, A. Prediction Model of Fade Duration Statistics for Satellite Communications at Ka and Q bands. *IEEE Trans. Antennas Propag.* **2019**, *67*, 5519–5531. [CrossRef]
13. Pimienta-del-Valle, D.; Riera, J.M.; Garcia-del-Pino, P.; Siles, G.A. Alphasat Experiment in Madrid: Modeling Considerations on Fade and Inter–Fade Durations. In Proceedings of the 12th European Conference on Antennas and Propagation (EuCAP 2018), London, UK, 9–13 April 2018. [CrossRef]
14. Badron, K.; Ismail, A.F.; Din, J.; Tharek, A.R. Rain induced attenuation studies for V–band satellite communication in tropical region. *J. Atmos. Sol.-Terr. Phys.* **2011**, *73*, 601–610. [CrossRef]

15. Chakraborty, S.; Verma, P.; Paudel, B.; Shukla, A.; Das, S. Validation of Synthetic Storm Technique for Rain Attenuation Prediction Over High–Rainfall Tropical Region. *IEEE Geosci. Remote Sens. Lett.* **2021**, *19*, 1–4. [CrossRef]
16. Mandeep, J.S. Fade duration statistics for Ku–band satellite links. *Adv. Space Res.* **2013**, *52*, 445–450. [CrossRef]
17. Dao, H.; Al-Khateeb, K.; Al-Khateeb, K.; Ismail, A.F. Analysis of rain fade duration over satellite–earth path at Ku–Band in tropics. In Proceedings of the 2012 International Conference on Computer and Communication Engineering (ICCCE), Kuala Lumpur, Malaysia, 3–5 July 2012. [CrossRef]
18. García-del-Pino, P.; Riera, J.-M.; Benarroch, A. Fade and interfade duration statistics on an Earth–space link at 50 GHz. *IET Microw. Antennas Propag.* **2011**, *5*, 790–794. [CrossRef]
19. Cheffena, M.; Tjelta, T.; Breivik, T.O. Fade duration statistics of millimetre wavelength terrestrial line–of–sight links. In Proceedings of the Fourth European Conference on Antennas and Propagation, Barcelona, Spain, 12–16 April 2010; pp. 1–5.
20. Boulanger, X.; Gabard, B.; Casadebaig, L.; Castanet, L. Four Years of Total Attenuation Statistics of Earth–Space Propagation Experiments at Ka–Band in Toulouse. *IEEE Trans. Antennas Propag.* **2015**, *63*, 2203–2214. [CrossRef]
21. Nandi, D.; Pérez-Fontán, F.; Pastoriza–Santos, V.; Machado, M. Analysis of rain fade characteristics from experimental satellite measurements at Ka/Q bands for a temperate location Vigo, Spain. *Adv. Space Res.* **2021**, *68*, 1754–1760. [CrossRef]
22. Jong, S.L.; Riva, C.; D'Amico, M.; Lam, H.Y.; Yunus, M.M.; Din, J. Performance of synthetic storm technique in estimating fade dynamics in equatorial Malaysia. *Int. J. Satell. Commun. Netw.* **2018**, *36*, 416–426. [CrossRef]
23. Garcia-Rubia, J.M.; Riera, J.M.; Garcia-del-Pino, P.; Pimienta-del-Valle, D.; Siles, G.A. Fade and Interfade Duration Characteristics in a Slant–Path *Ka*–Band Link. *IEEE Trans. Antennas Propag.* **2017**, *65*, 7198–7206. [CrossRef]
24. Chakraborty, S.; Chakraborty, M.; Das, S. Second order experimental statistics of rain attenuation at Ka band in a tropical location. *Adv. Space Res.* **2012**, *67*, 4043–4053. [CrossRef]
25. Nandi, A. Prediction of Rain Attenuation Statistics from Measured Rain Rate Statistics using Synthetic Storm Technique for Micro and Millimeter Wave Communication Systems. In Proceedings of the 2018 IEEE MTT—S International Microwave and RF Conference (IMaRC), Kolkata, India, 28—30 November 2018.
26. Papafragkakis, A.Z.; Kourogiorgas, C.I.; Panagopoulos, A.D.; Ventouras, S. Second Order Excess Attenuation Statistics in Athens, Greece at 19.701 GHz using ALPHASAT. In Proceedings of the 12th International Symposium on Communication Systems, Networks and Digital Signal Processing (CSNDSP), Porto, Portugal, 20–22 July 2020. [CrossRef]
27. Kelmendi, A.; Hrovat, A.; Mohorčič, M.; Švigelj, A. Alphasat Propagation Measurements at Ka and Q-Bands in Ljubljana: Three Years' Statistical Analysis. *IEEE Antennas Wirel. Propag. Lett.* **2021**, *20*, 174–178. [CrossRef]
28. Recommendation ITU-R P. 618-14. *Propagation Data and Prediction Methods Required for the Design of Earth–Space Telecommunication Systems*; ITU: Geneva, Switzerland, 2023; Volume 8.
29. Matricciani, E. Prediction of fade duration due to rain in satellite communication systems. *Radio Sci.* **1997**, *22*, 935–941. [CrossRef]
30. Matricciani, E. Duration of rain–induced fades of signal from SIRIO at 11.6 GHz. *Electron. Lett.* **1981**, *17*, 29–30. [CrossRef]